



# LUND UNIVERSITY

## The Lund-York-Cologne Calorimeter (LYCCA): Concept, Design and Prototype Developments for a FAIR-NUSTAR Detector System to Discriminate Relativistic Heavy-ion Reaction Products

Golubev, Pavel; Wendt, A.; Scruton, L.; Taprogge, J.; Rudolph, Dirk; Reiter, P.; Bentley, M. A.; Avdeichikov, Vladimir; Boutachkov, P.; Fox, S. P.; Gerl, J.; Goergen, Ch.; Hoischen, Robert; Kurz, N.; Singh, B. S. Nara; Pascovici, G.; Pietri, S.; Schaffner, H.; Taylor, M. J.; Thiel, S.; Wollersheim, H. J.

*Published in:*

Nuclear Instruments & Methods in Physics Research. Section A: Accelerators, Spectrometers, Detectors, and Associated Equipment

*DOI:*

[10.1016/j.nima.2013.04.058](https://doi.org/10.1016/j.nima.2013.04.058)

2013

[Link to publication](#)

*Citation for published version (APA):*

Golubev, P., Wendt, A., Scruton, L., Taprogge, J., Rudolph, D., Reiter, P., Bentley, M. A., Avdeichikov, V., Boutachkov, P., Fox, S. P., Gerl, J., Goergen, C., Hoischen, R., Kurz, N., Singh, B. S. N., Pascovici, G., Pietri, S., Schaffner, H., Taylor, M. J., ... Wollersheim, H. J. (2013). The Lund-York-Cologne Calorimeter (LYCCA): Concept, Design and Prototype Developments for a FAIR-NUSTAR Detector System to Discriminate Relativistic Heavy-ion Reaction Products. *Nuclear Instruments & Methods in Physics Research. Section A: Accelerators, Spectrometers, Detectors, and Associated Equipment*, 723, 55-66. <https://doi.org/10.1016/j.nima.2013.04.058>

*Total number of authors:*

21

### General rights

Unless other specific re-use rights are stated the following general rights apply:

Copyright and moral rights for the publications made accessible in the public portal are retained by the authors and/or other copyright owners and it is a condition of accessing publications that users recognise and abide by the legal requirements associated with these rights.

- Users may download and print one copy of any publication from the public portal for the purpose of private study or research.
- You may not further distribute the material or use it for any profit-making activity or commercial gain
- You may freely distribute the URL identifying the publication in the public portal

Read more about Creative commons licenses: <https://creativecommons.org/licenses/>

### Take down policy

If you believe that this document breaches copyright please contact us providing details, and we will remove access to the work immediately and investigate your claim.

LUND UNIVERSITY

PO Box 117  
221 00 Lund  
+46 46-222 00 00



# LUND UNIVERSITY

Department of Physics

---

# LUP

Lund University Publications  
Institutional Repository of Lund University  
Found at: <http://www.lu.se>

This is an author produced version of a paper published in  
Nuclear Instruments and Methods in Physics Research A

This paper has been peer-reviewed but does not include the final  
publisher proof-corrections or journal pagination.

Citation for the published paper:

Author: P. Golubev *et al.*

Title: *The Lund–York–Cologne Calorimeter (LYCCA): Concept, design  
and prototype developments for a FAIR-NUSTAR detector system to  
discriminate relativistic heavy-ion reaction products*

Journal: Nucl. Instr. Meth. A 723, 55 (2013)

DOI: 10.1016/j.nima.2013.04.058

Access to the published version may require subscription.

# The Lund-York-Cologne Calorimeter (LYCCA): Concept, design and prototype developments for a FAIR-NUSTAR detector system to discriminate relativistic heavy-ion reaction products

P. Golubev<sup>a</sup>, A. Wendt<sup>b</sup>, L. Scruton<sup>c</sup>, J. Taprogge<sup>1,2,b</sup>, D. Rudolph<sup>a</sup>, P. Reiter<sup>b</sup>, M.A. Bentley<sup>c</sup>, V. Avdeichikov<sup>a</sup>, P. Boutachkov<sup>d,e</sup>, S.P. Fox<sup>c</sup>, J. Gerl<sup>d</sup>, Ch. G6rger<sup>b</sup>, R. Hoischen<sup>3,a,d</sup>, N. Kurz<sup>d</sup>, B.S Nara Singh<sup>c</sup>, G. Pascovici<sup>b</sup>, S. Pietri<sup>d</sup>, H. Schaffner<sup>d</sup>, M.J. Taylor<sup>4,c</sup>, S. Thiel<sup>b</sup>, H.J. Wollersheim<sup>d</sup>

<sup>a</sup>Department of Physics, Lund University, SE-22100 Lund, Sweden

<sup>b</sup>Institut f6ur Kernphysik, Universit6at zu K6oln, D-50937 K6oln, Germany

<sup>c</sup>Department of Physics, University of York, York YO10 5DD, United Kingdom

<sup>d</sup>GSI Helmholtzzentrum f6ur Schwerionenforschung GmbH, D-64291 Darmstadt, Germany

<sup>e</sup>Institut f6ur Kernphysik, Technische Universit6at Darmstadt, D-64289 Darmstadt, Germany

---

## Abstract

The concept, design and prototype developments for the Lund-York-Cologne CALorimeter (LYCCA) is presented. LYCCA is a modular device for the NUClear STructure, Astrophysics and Reactions (NUSTAR) science pillar of the Facility for Antiproton and Ion Research (FAIR) at Darmstadt, Germany. LYCCA is designed to discriminate heavy ions produced in nuclear reactions induced by relativistic radioactive ion beams. Measurements of energy loss, total energy, and time-of-flight allows the derivation of proton number,  $Z$ , and mass number,  $A$ , of the reaction products. LYCCA-inherent tracking of the flight paths of the reaction products enables coincident HIGH-resolution in-beam  $\gamma$ -ray SPECTroscopy (HISPEC) of atomic nuclei far from the line of  $\beta$ -stability.

*Keywords:* relativistic heavy ions, nuclear structure, time of flight, energy loss, total energy,  $A$  and  $Z$  identification

---

## 1. Introduction and Requirements

The NUClear STructure, Astrophysics and Reactions (NUSTAR) science pillar [1] of the Facility for Antiproton and Ion Research (FAIR) at Darmstadt, Germany awaits beams of relativistic radioactive ions with unprecedented intensities. The major incentive is to study the atomic nucleus at its extremes of proton-to-neutron ratio, which is of immediate relevance towards and motivated by heavy-element production in the course of stellar evolution.

The HIGH-resolution in-beam SPECTroscopy (HISPEC) [2] experiment within NUSTAR addresses nuclear structure questions by using radioactive beams to be delivered by the new, super-conducting FRagment Separator (Super-FRS) [3]. The beam energies are typically some 100-300 MeV/u. Single-step Coulomb excitation and nuclear fragmentation reactions at these intermediate energies as well as inelastic scattering, transfer and knock-out reactions are envisaged. The experiments

will provide information relevant for the shell structure of atomic nuclei far from the line of  $\beta$ -stability, and more specifically low-lying excitation energies, transition probabilities, or single-particle spectroscopic factors, to name but a few.

The core of HISPEC is the use of high-resolution Ge detectors at one of the focal planes of the Super-FRS, i.e. to perform high-resolution in-beam spectroscopy of excited nuclear quantum states via their  $\gamma$ -ray decay; therefore, the HISPEC set-up foresees at its core the European Advanced GAMMA-ray Tracking Array (AGATA) [4], surrounding the secondary target position. To enable event-by-event correlations of the  $\gamma$  rays with the nuclear residues, HISPEC will comprise a new generation of beam tracking and identification detectors placed in front of and behind the secondary target. Here, the Lund-York-Cologne CALorimeter (LYCCA) has the central role of determining both proton number,  $Z$ , and mass number,  $A$ , of the final reaction products; by itself or in conjunction with a magnetic spectrometer. Until HISPEC becomes operational, a subset of LYCCA detectors is being commissioned and used for

---

*Email address:* Pavel.Golubev@nuclear.lu.se (P. Golubev)

the PRESPEC-AGATA [5] physics campaign at the existing FRS facility [6] at the GSI Helmholtzcentre for Heavy Ion Research in Darmstadt, Germany.

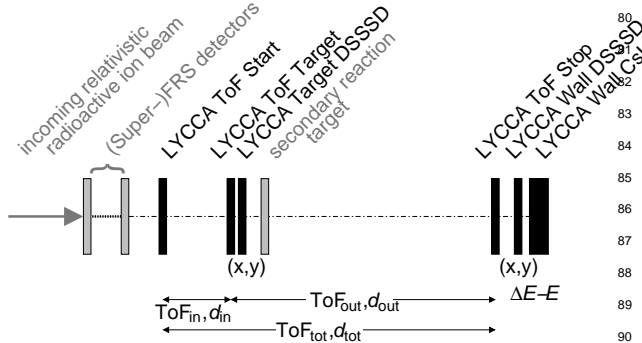


Figure 1: Sketch of the detection concept of LYCCA. LYCCA-related items are drawn in black. See text for details.

HISPEC-type experiments have also been performed already within the Rare Isotope Spectroscopic Investigations at GSI (RISING) Fast-Beam campaign 2003–2005 [7]. Here,  $\gamma$ -ray spectroscopy with fifteen former EUROBALL Cluster detectors [8] was performed in conjunction with the CALorimeter TElescope (CATE) [9], which at the time provided discrimination between nuclear reaction products. Both the experience with CATE and extensive simulations within the LYCCA collaboration [10] show that several items are essential for an improved HISPEC calorimeter system:

- A physical segmentation of both  $\Delta E$  and  $E$  elements is useful for both rate considerations and active tracking.
- To achieve a proper mass separation, a high-precision time-of-flight system (better than 50 ps FWHM resolution [10]) needs to be integrated.
- LYCCA should be able to deal with rather light nuclei,  $A \sim 30$ , at energies up to 300 MeV/u, likewise heavy nuclei,  $A \sim 200$ , down to about 100 MeV/u.

The resulting LYCCA detection concept within the HISPEC framework is sketched in Fig. 1: Up front, the definition of the tracked position and proton number,  $Z$ , as well as mass number,  $A$ , of the incoming relativistic radioactive ion beam is subject to either future Super-FRS or existing FRS detection systems. A double-sided silicon strip detector (DSSSD) at the secondary target position together with those forming the downstream LYCCA wall ensure precise  $(x,y)$ -tracking of the reaction products. At the same time, the DSSSD wall ele-

ments provide an energy-loss signal,  $\Delta E$ , which in conjunction with the measurement of the residual energy,  $E_{res}$ , of the recoiling reaction products aims at determining their proton number,  $Z$ , by means of the established  $\Delta E$ - $E_{res}$  technique.  $E_{res}$  is determined by LYCCA wall CsI(Tl) detector elements. The DSSSD position measurement also has the capacity to improve CsI energy resolution through straightforward corrections of possible CsI light-collection dependencies on the impact position of the ions.

To determine the mass number,  $A$ , of the reaction products,  $E_{res}$  is being correlated with time-of-flight (ToF) information (cf. Ref. [10]), in particular by measuring  $ToF_{out}$  over the distance  $d_{out}$  between the LYCCA ToF Target and LYCCA ToF Stop detectors. The thickness of the secondary target used in previous in-beam campaigns seriously limited the envisaged mass resolution of the CATE spectrometer. This was especially worsened in fragmentation reactions due to the momentum spread induced by the reaction process. Therefore, available flight-paths and required solid-angle coverage call for a high-precision timing measurement. Simulations indicate [10] that a timing resolution of 50 ps (FWHM) or better is required, though this number depends on recoil energies and the mass regimes of interest. The ToF Target detector is placed near the secondary target inside the target chamber, the ToF Stop detector close to the LYCCA wall DSSSD elements. In addition, the individual velocities of incoming beam particles can be re-determined with  $ToF_{in}$  between the LYCCA ToF Start and LYCCA ToF Target detector over the distance  $d_{in}$ .

Based on the LYCCA simulations [10] and anticipated typical HISPEC experiments and experimental conditions, the following design goals concerning  $A$  and  $Z$  resolution of LYCCA have been defined in the LYCCA Technical Design Report [11]:

DSSSD energy resolution (FWHM) at 0.1 GeV:

$\Delta E/E < 1\%$ , projected goal  $\Delta E/E < 0.5\%$

CsI(Tl) energy resolution (FWHM) at 10 GeV:

$\Delta E/E < 1\%$ , projected goal  $\Delta E/E < 0.5\%$

ToF resolution (FWHM):

$\Delta t < 100$  ps, projected goal  $\Delta t < 50$  ps

In principle, these numbers are considered initial guidelines, while the actual LYCCA performance depends strongly on the available flight paths and experimental parameters, namely the mass regimes to be studied, secondary target thickness, or the focussing scheme of a relevant (Super-)FRS setting.

Section 2 details the various detector components of LYCCA. A brief description of the mechanical housing of the LYCCA wall  $\Delta E$ - $E_{res}$  telescopes in Sec. 3 is fol-

lowed by a brief overview of hitherto used processing and read-out electronics in Sec. 4. Section 5 illustrates very first in-beam commissioning spectra of LYCCA, thereby confirming the achievement of the design goals indicated above. The paper concludes with an outlook towards LYCCA as a FAIR-NUSTAR detection device.

## 2. The LYCCA Detector Components

### 2.1. The Target DSSSD

Double sided silicon strip detectors (DSSSD) are common in physics experiments as an apparatus to measure the energy loss,  $\Delta E$ , and position,  $(x,y)$ , of particles passing through the silicon bulk of the detectors. The silicon wafers used as LYCCA target DSSSDs are ion implanted, silicondioxide ( $\text{SiO}_2$ ) passivated, and operated totally depleted with floating guard rings. They are obtained from RADCON Limited.

The nominally 300-320  $\mu\text{m}$  thick wafers are square shaped, 60.1 mm  $\times$  60.1 mm in size with an active area of 58.5 mm  $\times$  58.5 mm. The active area is subdivided into 32 strips on both front (junction) p-side and rear (ohmic) n-side in orthogonal directions providing two dimensional position information. With 58.5 mm/32=1.83 mm, the pitch of the p-side strips is 1.80 mm with an interstrip  $\text{SiO}_2$  isolation of 30  $\mu\text{m}$ . To improve interstrip capacitive and resistive isolation from the adjacent n-strips on the ohmic side, a so-called p-type zone or p-stop structure surrounding n-strips was implanted. Thus the pitch size on the ohmic side is 1.63 mm with interstrip distances of 200  $\mu\text{m}$ .

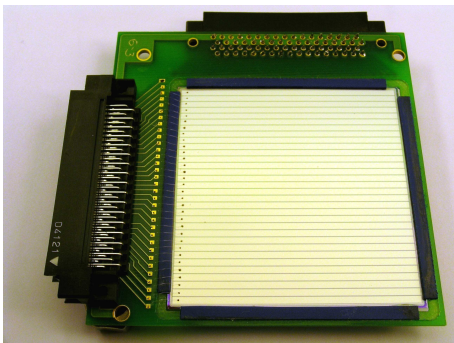


Figure 2: Photograph of a target DSSSD detector.

Leakage currents, upon delivery, range between 5-10 nA per strip with modest capacities of 33 pF per strip at full depletion voltage, which is typically reached at 50 V. The energy resolution and crosstalk was measured by scanning detectors with collimated  $^{228}\text{Th}$  and  $^{241}\text{Am}$   $\alpha$ -particle sources. A typical spectrum for this type of

DSSSD, obtained in a test chamber using standard LYCCA vacuum feedthrough, cabling, and electronics (see Secs. 3 and 4), is shown in Fig. 5(a).

The thickness of the dead layers on both sides of detectors was determined by measuring the energy loss of the  $\alpha$  particles by irradiating the detector from different incident angles. They are found to be  $\sim 1.0 \mu\text{m}$  Si-equivalent on the junction side and  $\sim 2.0 \mu\text{m}$  on the ohmic side. To optimize charge collection on the rear side of the detector the full depletion voltage was measured by injecting  $\alpha$  particles into the ohmic side and maximizing detector response as a function of applied bias voltage.

The target DSSSD is mounted on a printed circuit board made of FR4 together with connectors and gold plated pads for strips bonding. Due to possible harsh radiation damage all components and material used for detector packaging allow temperature annealing at low-to-medium temperature for few days. The detector frame is mechanically compatible for mounting into the secondary reaction chamber together with the ToF Target detectors (cf. Secs. 2.3.2 and 2.3.3) and various secondary reaction targets.

### 2.2. The LYCCA $\Delta E$ - $E_{\text{res}}$ Wall Telescope

The requirements described in Sec. 1 call for the use of telescopes based on segmented semiconductor detectors backed by segmented inorganic scintillators read-out by photodiodes (PD). Such a device presents a powerful tool for charged particle identification in a wide range of charge, mass, and energy, the latter if being used to stop the particles. Due to the very broad range of experimental conditions for which LYCCA is constructed, a modular design was deemed necessary.

All modules are identical telescopes where particle identification is obtained through  $\Delta E$ - $E_{\text{res}}$  measurements. In addition, internal segmentation of the telescope components provides the capability to sustain sufficiently high counting rates as well as multiple particle detection even within one single telescope. In the following subsections the design, construction, test results, and performance of LYCCA telescopes are presented.

#### 2.2.1. The DSSSD Frame

For energy loss,  $\Delta E$ , measurements, each LYCCA telescope comprises a 300-320  $\mu\text{m}$  DSSSD as detailed in Sec. 2.1. To minimize physical dead areas surrounding each DSSSD, a very close packing of telescopes into the full LYCCA array is of high importance, thus a minimal amount of material for the DSSSD frame was a central design goal. The LYCCA solution is to mount

212 the silicon wafer into a thin frame made out of FR4  
 213 printed circuit board (PCB) material with the help of  
 214 custom made tools and a bonding assembly [12] based  
 215 on epoxy rubber CAF4 [13], which ensures the neces-  
 216 sary mechanical stability and elasticity for possible me-  
 217 chanical tensions on the frames. Only 0.2 mm of the de-  
 218 tector frame extends beyond the wafer on the two con-  
 219 nector free sides, and 2.0 mm on the two sides where  
 220 signal multipin connectors are mounted. The frame has  
 221 gold plated pads for bonding and pin-like connectors  
 222 (BLX-1-056-40G) soldered for signal extraction.

223 The challenge of minimal dead space of the tele-  
 224 scope front face and signal read-out combined with  
 225 mechanical stability for the subsequent heavy-weight  
 226 block of CsI(Tl) scintillators (see below) is overcome  
 227 by specially designed signal transportation boards. These  
 228 boards fabricated out of FR4 PCB material are equipped  
 229 at one edge with connectors (SLX-1-053-30G) to be at-  
 230 tached to the thin DSSSD frame. At the another end  
 231 of the signal transportation board multipin connectors  
 232 (KEL 8831E-068-170) are mounted for further DSSSD  
 233 signal transportation towards the feedthrough boards of  
 234 the LYCCA vacuum chamber. A closeup view of a  
 235 DSSSD mounted on its PCB frame and in combination  
 236 with the signal transportation boards assembly is shown  
 in Figs. 3(a) and (b), respectively.

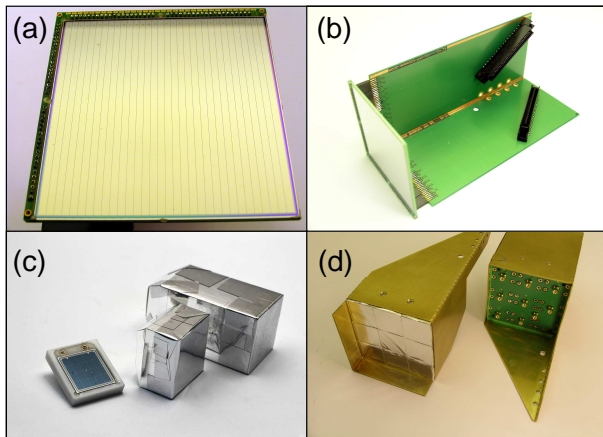


Figure 3: LYCCA module elements: (a) A DSSSD wafer mounted in its thin PCB frame and (b) coupled to the signal transport boards. (c) A photodiode mounted in its ceramic plate and CsI ‘short’ and ‘long’ crystals wrapped in the ESR reflecting foil. (d) A 9-element CsI-block in the brass frame.

237

### 238 2.2.2. The CsI Block

239 Each LYCCA telescope is equipped with an array of  
 240 nine CsI(Tl) crystals being placed 10 mm behind the  
 241 DSSSD wafer to measure the full residual energy,  $E_{res}$ ,

242 of the particles. The front face of all CsI(Tl) crystals has  
 243 the dimension  $19.4 \times 19.4 \text{ mm}^2$  and there are two dif-  
 244 ferent lengths of crystals available: a ‘long’ version of  
 245 33.0 mm in depth plus 7.0 mm of pyramidal lightguide  
 246 and a ‘short’ version of 10.0 mm in depth with 5.0 mm  
 247 pyramidal lightguide. The dimensions of the back end  
 248 of the pyramidal light guide are  $10.4 \times 10.4 \text{ mm}^2$  match-  
 249 ing the size of the read-out PDs.

The choice of CsI(Tl) is dictated by its high stopping  
 power, high light output, and the relatively easy hand-  
 ling of this type of inorganic scintillator. One of the  
 important characteristic of the CsI(Tl) crystal for high-  
 resolution charged-particle spectroscopy is light out-  
 put variations arising from possible gradients or local  
 fluctuations of the Tl concentration. To achieve opti-  
 mal light uniformity all crystals were machined from  
 a single ingot. The typical Tl concentration is 0.08-  
 0.10 mol%. All crystals were supplied by Amcryst-H  
 Ltd., Kharkov, Ukraine [14].

The achievable resolution of total energy measure-  
 ment depends first of all on non-uniformities of light  
 collection across the active volume of a CsI crystal.  
 Secondly, it depends on the position of energy depo-  
 sition but also on the deposited energy density. Such  
 aspects are detailed in Refs. [15, 16, 17]. For example,  
 light output depends strongly upon the reflecting mate-  
 rial used for wrapping. ESR film was proposed [18] and  
 also tested for LYCCA and found to be most optimal  
 for wrapping all sides of the crystals except for the front  
 face. The ESR foil is partially transparent in the blue re-  
 gion of scintillation light. To achieve optical isolation of  
 a crystal from its neighbours each crystal was addition-  
 ally wrapped into  $12 \mu\text{m}$  thin Al-foil. The same foil was  
 used to cover front face of the crystal to maximize light  
 collection from the scintillation process and at the same  
 time minimize dead layer for incoming particles. Fol-  
 lowing a number of cross checks, no additional lapping  
 to compensate for potential light non-uniformity along  
 the crystals appears needed, not least due to the rela-  
 tively small dimensions of the LYCCA CsI(Tl) crystals.

The scintillation light produced in the CsI(Tl) crys-  
 tals is read-out by photodiodes (PD). The PDs are  
 $10.6 \text{ mm} \times 11.6 \text{ mm} \times 0.3 \text{ mm}$  in size and supplied  
 by RADCON Ltd., Zelenograd, Russia. The PDs are  
 mounted into custom-made application specific ceramic  
 frames and glued directly onto the light guide of the  
 crystal by means of Epo-Tek 302 optical epoxy. The  
 chosen PD has a very good matching for the CsI(Tl)  
 scintillator emission light: the quantum efficiency is as  
 high as  $\sim 82\text{-}86\%$  at 560 nm, which is the peak po-  
 sition in the emission spectrum of the CsI(Tl). The total  
 spectral response of the PD ranges from 320 nm up to



294 1060 nm with a maximum at some 920 nm. At nomi- 322  
 295 nal operating voltage 35 V the leakage current is on the 323  
 296 level of 1-2 nA and the capacitance is 38-40 pF at full 324  
 297 depletion. 325

298 Nine CsI(Tl)-PD units are packed into a 3 × 3 ar- 326  
 299 ray into a brass frame which allows for proper relative 327  
 300 alignment of all active elements of a LYCCA telescope 328  
 301 (see below). A FR4 PCB CsI(Tl)-PD signal distribu- 329  
 302 tion board is soldered directly onto the nine PD's pins. 330  
 303 This board is also equipped with MMCX connectors, and 331  
 304 shielded coaxial cables are used for PD signal trans- 332  
 305 portation towards the feedthrough boards of the LYCCA 333  
 306 vacuum chamber to guarantee noise immunity and neg- 334  
 307 ligible signal cross talk. Figs. 3(c) and (d) provide pho- 335  
 tographs of various CsI(Tl) detector components. 336

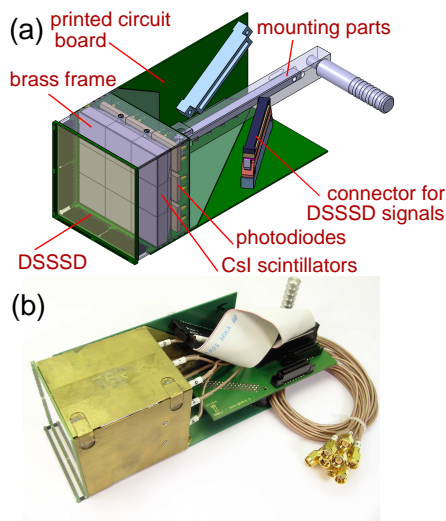


Figure 4: A LYCCA telescope (a) in its three-dimensional CAD drawing stage and (b) in its LYCCA-1 realization.

308

### 309 2.2.3. The LYCCA Module

310 The single LYCCA telescope module is made up of 311  
 312 one DSSSD mounted on its thin frame connected to the 313  
 314 signal transportation boards, with the brass frame of a 315  
 316 CsI scintillator block mechanically attached. Additionally, 317  
 318 a custom-made mechanical locking system for mounting the 319  
 320 telescope into LYCCA chamber (see Sec. 3) is linked to the 321  
 322 brass frame and the signal transportation boards. The detachable 323  
 324 nature of the CsI block allows easy access to both telescope 325  
 326 components and active elements for exchange, service or repair. 327  
 328 Figs. 4(a) and (b) provide both the technical drawing and a 329  
 330 photograph of a real LYCCA telescope. 331

332

### 333 2.2.4. Bench Tests

334 A test vacuum chamber has been configured to enable 335  
 336 high-resolution test measurements and overall performance 337  
 338 tests for LYCCA detectors. The test chamber is equipped with 339  
 340 mechanics, cables, connectors and front-end electronics identical 341  
 342 to items used in the real LYCCA chamber. Various radioactive 343  
 344 sources can be mounted inside the chamber to provide possibilities 345  
 346 for comprehensive detector testing. 347

348 The energy resolution and crosstalk for each DSSSD 349  
 350 was measured by scanning detectors with collimated 351  
 352  $^{228}\text{Th}$  and  $^{241}\text{Am}$   $\alpha$ -particle sources in the test chamber. 353  
 354 A typical spectrum, obtained using standard LY- 355  
 356 CCA electronics (cf. Sec. 4), vacuum feedthrough and 357  
 358 cabling is provided in Fig. 5(a). The pixel resolution has 359  
 a typical value of less than 50 keV FWHM at 9 MeV  $\alpha$  360  
 energy, which comprises also significant uncertainties 361  
 from source as well as deadlayer thicknesses. 362

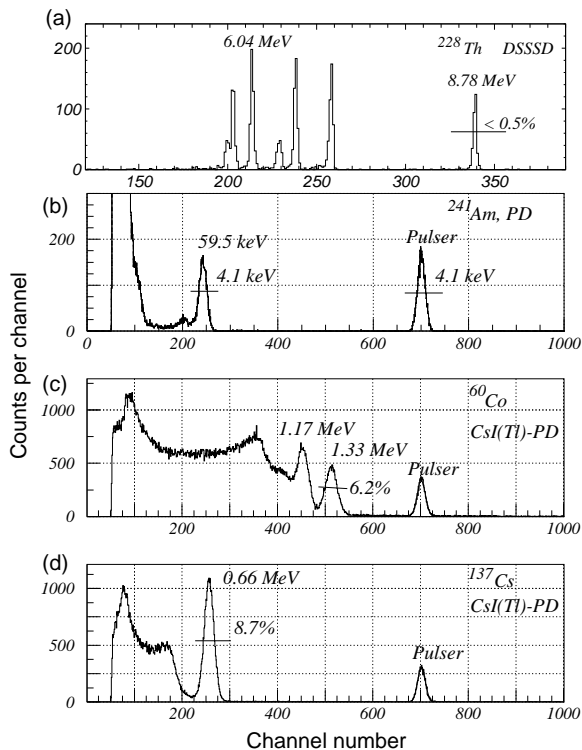


Figure 5: Energy calibration spectra for a bare photodiode (b), a CsI(Tl)-PD detector (b,c), and a LYCCA DSSSD detector (d). Energy resolutions are indicated and there are labels for the respective radioactive source used.

339 Standard  $\gamma$ -ray sources ( $^{60}\text{Co}$ ,  $^{137}\text{Cs}$ ,  $^{243}\text{Am}$ ) have 340  
 341 been used for various energy resolution measurements of bare 342  
 343 photodiodes, single CsI(Tl)-PD units, and complete CsI block 344  
 345 assemblies, respectively. Figs. 5(b)-(d) show some of these  $\gamma$ -ray 346  
 347 spectra. For example, the 348

345 energy resolution measured at  $E_\gamma = 1.3$  MeV yields  
 346 6.2% FWHM for the ‘short’ crystal version. Taking  
 347 into account the well known  $R \sim 1/\sqrt{E}$  power law re-  
 348 lation for energy resolution dominated by statistical ef-  
 349 fects one can anticipate that the projected goal is eas-  
 350 ily reached for an expected minimum deposited energy  
 351 of at least several GeV in CsI(Tl) crystals in real PRE-  
 352 SPEC or HISPEC experiments. Following the modules’  
 353 use in real experiments, spectra such as those displayed  
 354 in Fig. 5 serve as reference spectra for quality assess-  
 355 ment and maintenance procedures [19].

356 Successful tests of the first LYCCA prototype tele-  
 357 scope inside the test chamber performed with a proton  
 358 beam delivered by the Tandem Accelerator of the Uni-  
 359 versity of Cologne are summarized in Ref. [20].

360 Further calibration aspects for  $\Delta E$ - $E_{\text{res}}$  telescopes are  
 361 addressed in Refs. [21, 22] followed by in-beam tests  
 362 during the R&D phase of related DSSSD-CsI(Tl) tele-  
 363 scope arrangements [23].

### 364 2.3. The LYCCA ToF Detectors

365 The R&D of LYCCA ToF detectors has followed es-  
 366 sentially two lines (cf. Ref. [11]): A new class of large-  
 367 area scintillation membranes [24] and the development  
 368 of polycrystalline, chemical vapour deposited diamond  
 369 detector wafers [25]. In-beam commissioning experi-  
 370 ments have been successfully performed with both sys-  
 371 tems, while availability, performance, and also cost-per-  
 372 formance issues favour the scintillator concept, at  
 373 least within the LYCCA framework.

#### 374 2.3.1. The ToF Start and ToF Stop Elements

375 The ToF Start and ToF Stop detectors follow a new  
 376 design approach for large-area plastic scintillation de-  
 377 tectors: A circular membrane of Saint-Gobain BC-420  
 378 with 27 cm diameter is read out by 32 Hamamatsu  
 379 R7400U photomultiplier tubes. The R&D, components,  
 380 construction, and the in-beam result of an intrinsic de-  
 381 tector resolution of  $\Delta t \ll 50$  ps FWHM is detailed in  
 382 Ref. [24]. In brief, the unusually good timing resolution  
 383 for plastic scintillator systems is achieved through col-  
 384 lecting the light in 32 independent measurements. Tak-  
 385 ing an average, i.e. to first order by means of the factor  
 386  $1/\sqrt{32} \sim 0.2$ , results in a better effective ToF resolution  
 387 than other fast materials with a better intrinsic resolu-  
 388 tion such as, for example, diamond detectors.

#### 389 2.3.2. The ToF Target Scintillation Detector

390 Based on the achievements of the large membrane  
 391 scintillators, a smaller Target ToF scintillation detec-  
 392 tor with an active diameter of 73 mm has been de-  
 393 signed and built recently. This dimension follows (i) the

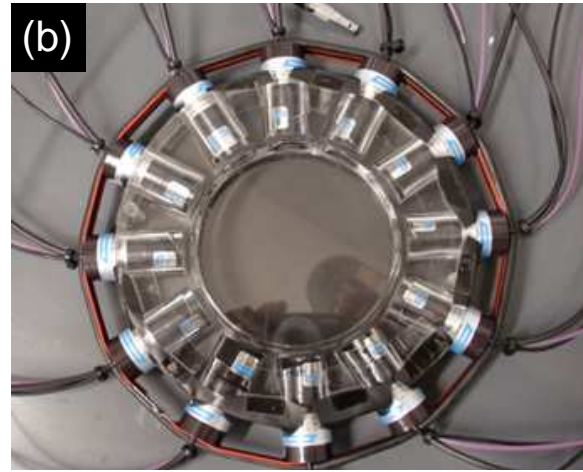
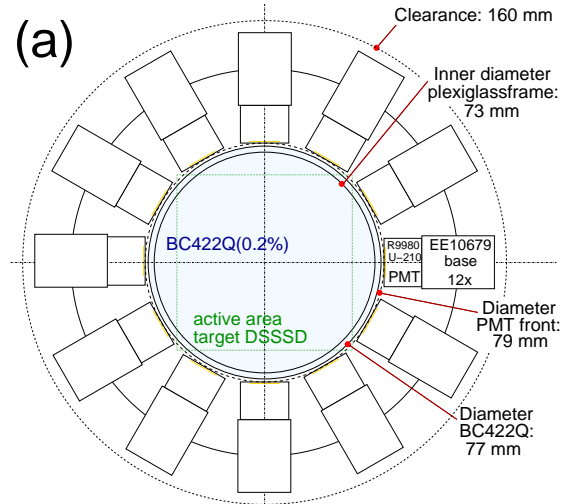


Figure 6: (a) Drawing of the LYCCA ToF Target detector and (b) photograph of its realization.

394 need for typical beam spot sizes of relativistic radioac-  
 395 tive ion beams at the secondary target position, namely  
 396  $\sigma_x \sim \sigma_y \sim 1.5$  cm, and (ii) the constraints by the size of  
 397 the HISPEC-AGATA vacuum chamber surrounding the  
 398 secondary target. Figure 6 provides a drawing and pho-  
 399 tograph of this detector. Simulations based on the stud-  
 400 ies in Refs. [24, 26] indicate that despite the necessarily  
 401 smaller number of only 12 photomultiplier tubes a time  
 402 resolution similar to the above can be achieved by using  
 403 quenched Saint-Gobain BC422Q(0.2%) instead of BC-  
 404 420 and by replacing the former Hamamatsu R7400U  
 405 tubes with the latest generation of Hamamatsu R9880-  
 406 210. A detailed performance characterisation of this  
 407 new detector is going to be a part of a comprehensive  
 408 subsequent publication on LYCCA in-beam measure-  
 409 ments [27].



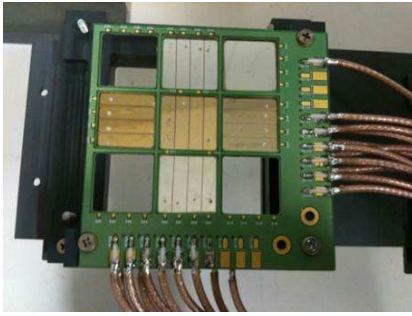


Figure 7: Photograph of the prototype of the LYCCA Target ToF diamond detector.

### 2.3.3. The ToF Target Diamond Detector

Any LYCCA ToF detector placed at the target position is required to cover the full area of the secondary target. This necessity led to the development of what we believe to be one of the largest area diamond detectors tested to date. As can be seen in figure 7, the detector can accommodate nine  $20 \times 20 \times 0.3 \text{ mm}^3$  polycrystalline diamond wafers formed by chemical vapour deposition, although only six were used for this experiment. Five of the wafers are segmented into four strips measuring  $18 \times 4.5 \text{ mm}^2$ . These wafers were mounted onto a custom-made PCB, allowing for separate biasing and signal extraction for each strip. The signals were amplified using 2.3 GHz broadband DBAIV preamplifiers [28], specially designed for fast pulses from diamond. Further details on the fabrication and development results from an earlier version of this diamond detector can be found in Ref. [25].

In-beam measurements were made with the large-area plastic start and stop scintillators, as well as the target diamond detector to enable detailed comparisons of their timing performance. The precision of the diamond - plastic stop ToF measurements were compared with the plastic start - plastic stop ToF measurements, which had flight paths of  $d_{\text{out}} = 3.61(1) \text{ m}$  and  $d_{\text{tot}} = 4.31(3) \text{ m}$ , respectively. Details of the latter can be found in Sec. 5. The same procedure applied to the diamond indicates a resolution of 193 ps (FWHM). This compares with the best result of 103 ps (FWHM), obtained at Texas A&M University [25] using the same configuration of diamond wafer.

Further analysis has concluded that this worsening of the resolution is likely to be caused by the necessarily large length of cable (2.5 m compared with 1 m at Texas A&M University) present between the diamond detector and the DBAIV, which significantly increased the capacitance on the input of the preamplifier. The charge collection from the detector was also found to be smaller

during the commissioning experiment. These factors would be expected to have adverse effects on the noise contribution to the final amplified signal, and the timing resolution would become worse as a result. Indeed, it should be noted that where diamond has demonstrated especially good timing resolution, the custom built electronics have always been adjacent to the detector [29].

From this it can be concluded that it will be challenging for diamond to meet the optimum resolution required for LYCCA without significant redesign of the signal processing arrangements. This, coupled to the better final resolution demonstrated by the plastic scintillators (cf. Sec. 5) has led the LYCCA collaboration to decide that the LYCCA ToF measurements for the final NUSTAR device should be undertaken using the plastic scintillation detectors.

## 3. The LYCCA Chamber

The mechanical construction to hold the LYCCA  $\Delta E - E_{\text{res}}$  modules (see Sec. 2.2.3 and Fig. 8(a)) is compatible with the final full LYCCA setup and flexible to be placed at any suitable position along the Super-FRS and HISPEC beamlines, provided rather trivial coupling flanges being manufactured in the future. In addition, the mechanical construction allows for a relatively easy replacement of single LYCCA  $\Delta E - E_{\text{res}}$  modules if deemed necessary from an experimental point of view.

The LYCCA-chamber itself is based on a cylindrical vacuum vessel with a diameter of 800 mm and a depth of 400 mm. The upstream side has an open circular entrance with a diameter of 450 mm for the incoming particles. The vacuum chamber is designed to host up to the anticipated 26 LYCCA  $\Delta E - E_{\text{res}}$  detector modules in 5 rows of 4, 6, 6, 6, and 4 modules each. The photograph on the right hand side of Fig. 8 shows the realization of the LYCCA vacuum chamber with  $3 \times 4$  LYCCA modules mounted. This represents the configuration used for the first PRESPEC experiments in 2010 and 2011. For the PRESPEC-AGATA experiments in 2012 and 2014, 4 additional modules were implemented, namely 2 in the centre of the top and 2 in the bottom row, respectively.

While fixed on top of a support table, the LYCCA vacuum vessel has a standard flange to connect to a vacuum pumping system at its bottom. Radially, some 70 vacuum feedthroughs are foreseen to carry the signals from detector elements inside the vacuum chamber into custom-made 32-channel preamplifiers (cf. Sec. 4.2) via glued-in printed circuit boards. Until 2014, this scheme is followed for both CsI and DSSSD detectors

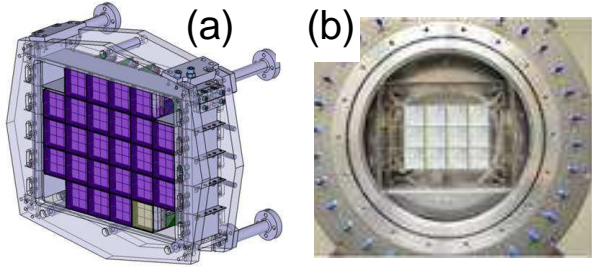


Figure 8: (a) Technical 3D drawing of the holding structure for LYCCA modules inside the LYCCA Wall vacuum chamber. (b) Photograph of the LYCCA Wall vacuum chamber as seen by the beam with twelve LYCCA modules mounted inside the holding structure.

(cf. Secs. 4 and 5). The preamplifiers connect via 68-pin high-density connectors and are mechanically oriented and held in place by means of a dedicated 'plug-and-play' mechanism. Hence, both electrical contacts and mechanical stability are secured while keeping the distance between detectors and preamplification stage minimal. Vacuum feedthroughs are also provided for temperature and pressure read-out.

For the complete PRESPEC experimental campaign 2010-2014, the LYCCA ToF Stop detector (cf. Sec. 2.3) is also contained in the main LYCCA Wall vacuum chamber. In fact, some of its signal- and high-voltage vacuum feedthroughs can be seen in Fig. 8(b). For HISPEC, a revised and further optimized LYCCA ToF Stop plastic scintillation detector, covering the complete area of all 26  $\Delta E$ - $E_{\text{res}}$  modules, is being manufactured. This detector is going to be inside a separate vacuum housing in front of the existing LYCCA Wall vacuum chamber.

More comprehensive information on the LYCCA vacuum chamber is provided in Refs. [11, 20, 30, 31].

## 4. LYCCA Electronics

### 4.1. Processing of LYCCA ToF Detector Signals

The processing of the signals of the photomultiplier tubes of the LYCCA ToF system based on plastic scintillators is detailed in Ref. [24]. In short, the outputs of the photomultiplier bases are directly plugged into 5-channel Phillips Scientific Model 715 constant fraction discriminators [32]. Commercial time-to-digital converters CAEN V1290A, providing 21-bit dynamic range and 25-ps time bins, are used to digitize the individual timing signal with respect to a common reference, namely the accepted event trigger signal of the complete PRESPEC data acquisition system. Once in place, the 12 timing signals of the Target ToF detector are also put into a logic OR unit to provide an optional 'Target ToF'

trigger input signal. The remotely controllable high-voltage supply to the photomultiplier bases comprises four 16-channel ISEG EH160-30n305SHV modules in a common main frame [33].

A similar electronics scheme was also used for the target diamond detector. The outputs of the DBAIV preamplifiers were fed into Phillips Scientific Model 708 leading edge discriminators [32], and then converted into ECL signals and passed into the same CAEN V1290A TDC. Each strip on the diamond detector was biased to 395 V, which was applied via the DBAIV preamplifiers. Further details can be found in Ref. [25].

### 4.2. The 32-channel LYCCA preamplifier

Within the framework of the LYCCA project, the CSP-32(X) series of highly compact, charge-sensitive preamplifiers was developed at the University of Cologne. The underlying design is such that in principle a wide energy range of the signals from both DSSSDs and PDs is covered, with an easily reconfigurable amplification stage up to a 10 GeV range. For LYCCA the model CSP-32(4.1GeV) is selected from this series [11], which foresees a switchable dynamic range between 1.3 GeV and 4.1 GeV. An overview of the main components of the CSP-32(4.1GeV) is presented in Fig. 9. It consists of the following stages:

- a charge-sensitive loop with frequency compensations,
- a passive pole-zero cancellation and attenuation stage, and
- a balanced differential output buffer.

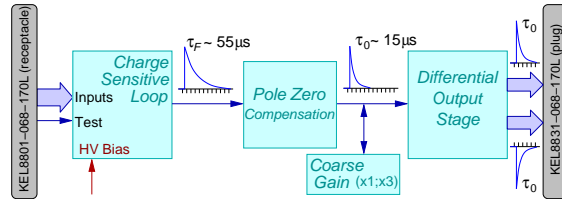


Figure 9: Block diagram of one channel of the front-end electronics for DSSSD and photodiode processing of LYCCA modules. Fall times of  $\tau_F \sim 55 \mu\text{s}$  after the first amplification stage and  $\tau_0 \sim 15 \mu\text{s}$  following pole zero compensation are indicated.

The charge sensitive loop has a conversion factor of 50 pC/V. It comprises an input stage with a very low noise jFET transistor, a current feedback operational amplifier, a passive feedback circuitry and a rather complex frequency compensation network. The use of a large feedback capacitance was mandatory to achieve

568 the large dynamic range but moreover to account for  
 569 placement of the detectors in a relatively large reaction  
 570 chamber, which implies long wiring between detector  
 571 elements and the charge sensitive preamplifier input cir-  
 572 cuitry. In order to cope with these adverse conditions  
 573 and to get a transfer function with a flat amplitude re-  
 574 sponse at the highest possible bandwidth, a multiple fre-  
 575 quency compensation network was designed and imple-  
 576 mented.

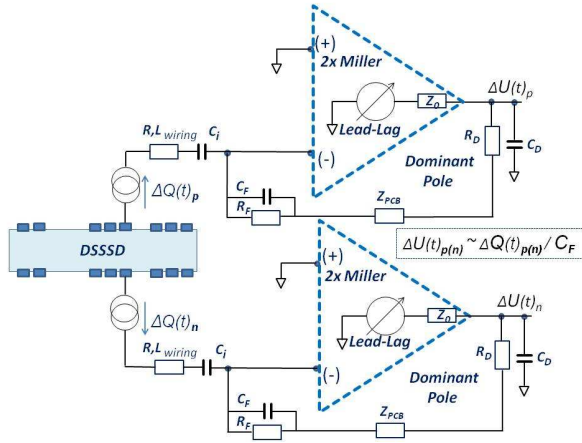


Figure 10: Simplified block diagram of the equivalent transimpedance amplifier stages and frequency compensation networks.

577 The connection of the detector elements to the  
 578 charge-sensitive loop input stage is AC (10 nF/400 V).  
 579 This is imposed by the required detector bias voltage  
 580 of up to 200 V. The choice of the preamplifier input  
 581 jFET type is one critical issue of such developments.  
 582 After some tests performed, we have found that the n-  
 583 channel jFET models BF861A and BF861C manufac-  
 584 tured by NXP Semiconductor represent the most ade-  
 585 quate choice. In fact, both provide a very low-noise  
 586 with a working point at a drain voltage of only  $\sim 2.0$ - $2.5$  V  
 587 and a drain current of less than 4 mA, i.e. a power con-  
 588 sumption of only  $\sim 8$ - $10$  mW.

589 The transimpedance amplifier of the charge sensitive  
 590 loop is built around a miniature current feedback opera-  
 591 tional amplifier (AD8005ART; RT-5 package) which  
 592 is showing a wide signal bandwidth (270 MHz), very  
 593 low quiescent current (typically 400  $\mu$ A) and at the  
 594 same time very low input voltage noise (4.0 nV/  $\sqrt{\text{Hz}}$  at  
 595 10 MHz). To match the different detector requirements  
 596 the feedback network values can vary for different con-  
 597 figurations: For LYCCA DSSSD detectors, the default  
 598 values are  $C_F = 56$  pF and  $R_L = 10$  M $\Omega$ , respectively  
 599  $\tau_F \sim 56$   $\mu$ s (Fig. 9).

600 The frequency compensation circuit is implemented  
 601 in the charge sensitive loop and it is similar to the  
 602 AGATA FEE design [34]. It comprises three main com-  
 603 ponents, namely one high-pass filter (as the Miller ef-  
 604 fect like internal compensations of the equivalent op-  
 605 erational amplifiers), one lead-lag filter, and finally one  
 606 dominant-pole compensation circuit. The lead-lag com-  
 607 pensation with a time constant of  $\sim 3$ - $5$  ns is a rather  
 608 high frequency compensation without sacrificing the  
 609 close-loop gain performance.

610 The dominant pole frequency compensation circuit  
 611 detailed in Fig. 10 compensates the pole existing in the  
 612 more complex feedback network of the charge sensitive  
 613 stage [35]. One takes advantage of the very large open  
 614 loop gain of the charge sensitive stage and its quite small  
 615 output impedance,  $Z_0$ , capable to drive the rather large  
 616 output capacitor of 10-20 pF. This network has a time  
 617 constant of  $\sim 1.0$ - $1.5$  ns and acts efficiently as a domi-  
 618 nant pole compensation without causing instabilities in  
 619 interaction with the intrinsic equivalent operational am-  
 620 plifier pole.

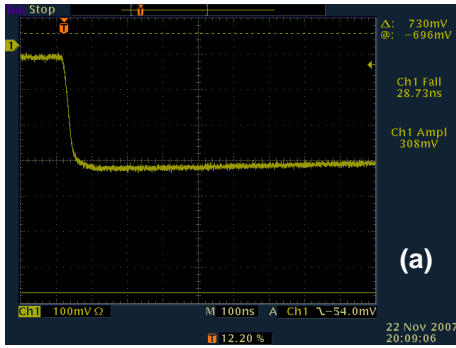
621 The rise time,  $t_{rise}$ , of the charge sensitive stage is  
 622  $\sim 13$  ns for zero input capacitance,  $C_{in} = 0$  pF, with  
 623 the rise-time slope being 0.3 ns/pF with almost no over-  
 624 shoot or undershoot over the whole dynamic range. A  
 625 typical transfer function in time domain for  $C_{in} \sim 60$  pF  
 626 and a step function as input test signal with  $t_{rise} \sim 1$  ns  
 627 is shown in Fig. 11(a).

628 To obtain similar fall-time characteristics of the out-  
 629 put signals for different dynamic range configurations of  
 630 the CSP-32(X) series, a pole-zero cancellation network  
 631 is also required, as shown in Fig. 9. By default the fall  
 632 time of the output signals is  $\sim 15$   $\mu$ s.

633 A differential signal transmission mode is chosen  
 634 to enhance the rejection to common-mode noise and  
 635 potential disturbances picked up along the output cable.  
 636 A balanced differential output stage has been de-  
 637 signed around the AD8012AR dual operational ampli-  
 638 fier which features low noise, low power, and wide  
 639 bandwidth. Only  $\pm 6$  V power supply has been chosen  
 640 due to the overall power consumption limitation of the  
 641 32 channels packed in a relatively small metal case of  
 642 80 mm  $\times$  40 mm  $\times$  120 mm in size. A photograph of an  
 643 open case is provided in Fig. 11(b).

644 The main specifications of the CSP-32(4.1GeV) can  
 645 be summarized as follows:

- 646 • conversion gain of the CSP stage 800 mV/GeV(Si),
- 647 • noise  $\sim 2.8$  keV FWHM ( $C_{detector} \sim 0$  pF),
- 648 • noise slope 11 eV/pF,



(b)

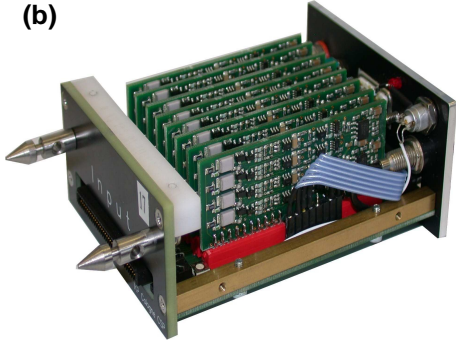


Figure 11: (a) Transfer function in time domain for a test with a step function as input signal with  $t_{rise} \sim 1$  ns. (b) View of the CSP-32 charge-sensitive preamplifier (box opened). 8 boards are visible, each equipped with 4 channels.

- 649 • rise time  $\sim 10$  ns,
- 650 • rise-time slope  $0.3$  ns/pF,
- 651 • fall time  $\sim 15 \mu\text{s}$  by default, while it can optionally
- 652 be factory adjusted in the range of  $10$ - $50 \mu\text{s}$ ,
- 653 • a switchable coarse gain of  $1/1$  or  $1/3$  is imple-
- 654 mented,
- 655 • differential output signals (with  $100 \Omega$  differential
- 656 output impedance and a dynamic range of  $\pm 4.5$  V-
- 657 terminated, here corresponding to the  $4.1$  GeV
- 658 range),
- 659 • overshoots/undershoots less than  $2.5\%$  over the
- 660 whole dynamic range.
- 661 • the 32 output signals can be directly digitized with
- 662 two GSI-EE 16-channel FEBEX3 sampling ADC
- 663 modules [38]

664 Last but not least, cross talk between detector channels  
 665 has to be considered in a complex detector system  
 666 where the sensor itself is highly segmented. Special  
 667 care has been taken to minimize the cross talk between

668 segments and between detectors at the level of the re-  
 669 action chamber ensemble set-up. To avoid additional  
 670 crosstalk between LYCCA detector elements, separated  
 671 return ground paths for each individual segment are pro-  
 672 vided, while the inductivities to the segment electrode  
 673 within the detectors wiring cannot be omitted.

#### 674 4.3. Processing of LYCCA DSSSD and CsI Elements

675 Until the final LYCCA read-out scheme based on  
 676 highly integrated and fully digitized preamplifier signals  
 677 [11] becomes operational within the FAIR-NUSTAR  
 678 data acquisition environment, an intermediate path based  
 679 on readily available and reasonably affordable inte-  
 680 grated electronics modules has been followed.

681 Each of the 32 signals from the p-side and the n-side  
 682 of the Target DSSSD are handled by one 32-channel  
 683 preamplifier box described in the previous Sec. 4.2. Six-  
 684 teen channels of differential preamplifier output are car-  
 685 ried by shielded twisted pair cable towards a total of  
 686 four single-unit NIM, 16-channel analogue shapers of  
 687 type Mesytec STM16 or MSCF16 [36]. The in total  
 688 64 energy channels are subsequently digitized by two  
 689 CAEN 785 peak-sensing analogue-to-digital converters  
 690 (ADC), the corresponding times of the 32 p-side chan-  
 691 nels measured by a CAEN 775 time-to-digital converter  
 692 (TDC) relative to the accepted event trigger. A logic  
 693 OR of all 64 timing channels can be used as an optional  
 694 'Target DSSSD' trigger input signal.

695 During the 2010-2011 PRESPEC experimental cam-  
 696 paign the four DSSSDs in the centre row of LY-  
 697 CCA modules [cf. Fig. 8(b)] were processed in an al-  
 698 most identical fashion: 8 custom-made preamplifiers  
 699 (cf. Sec. 4.2), hence 16 analogue shapers coupled to 8  
 700 ADCs were used, while the 128 timing signals of the p-  
 701 sides were digitized by a 128-channel CAEN 767 TDC.  
 702 The signals of the remaining 8 DSSSDs were combined  
 703 in units of four strips inside the LYCCA vacuum cham-  
 704 ber, which gives rise to additional  $8 \cdot (32+32)/4 = 128$  sil-  
 705 icon channels, i.e. four more preamplifiers, eight more  
 706 analogue shapers, four more ADCs, as well as a second  
 707 CAEN 767 TDC.

708 During the 2012-2014 PRESPEC-AGATA experi-  
 709 mental campaign, a total of 16 LYCCA  $\Delta E$ - $E_{res}$  mod-  
 710 ules are in use. Here, two neighbouring signals of all  
 711 DSSSDs are joined inside the LYCCA vacuum cham-  
 712 ber, which yields a total of  $16 \cdot (32+32)/2 = 512$  sil-  
 713 icon channels. These 512 channels are handled by 16 pre-  
 714 amplifiers, 32 analogue shapers, 16 ADCs, and two CAEN  
 715 767 TDCs, since still only the times of the p-sides of the  
 716 DSSSDs are being recorded. In both configurations, a  
 717 logic OR of all DSSSD p-side timing channels could or



718 can be used as an optional 'Wall DSSSD' trigger input  
719 signal.

720 The photodiode read-out of the CsI detectors in  
721 the LYCCA modules is handled very similarly: The  
722 modules are grouped together in units of three, such  
723 that  $3 \times 9 = 27$  photodiodes can be processed by one 32-  
724 channel preamplifier (identical to the one used for the  
725 DSSSDs, cf. Sec. 4.2), two analogue shapers, one ADC,  
726 and 32 channels of either a CAEN 775 TDC or part of  
727 a CAEN 767 TDC. A logic OR of all timing signals  
728 could or can be used as an optional 'Wall CsI' trigger  
729 input signal.

730 The high-voltage bias supply to both DSSSDs and  
731 photodiodes is provided by a set of four 4-channel  
732 Mesytec MHV4 NIM modules [36]. Remote control of  
733 MHV4 voltages as well as STM16/MSCF16 gain and  
734 threshold settings are enabled by two Mesytec MRC1  
735 slow-control units [36].

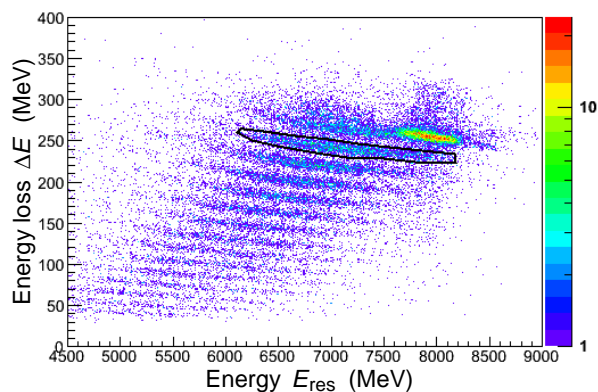


Figure 12: Energy loss vs. energy plot showing the Z distribution measured in one LYCCA  $\Delta E - E_{res}$  module. The Z = 26 selection for Fe fragments is shown.

## 736 5. First In-beam Commissioning Results

737 The first in-beam commissioning experiment for LY-  
738 CCA took place in September 2010, which aimed to de-  
739 termine the performance of the LYCCA detectors for  
740 nuclei around  $A \sim 60$ . A 550 MeV/u  $^{64}\text{Ni}$  beam was in-  
741 cident upon a 4 g/cm<sup>2</sup> thick  $^9\text{Be}$  production target at the  
742 entrance window to the FRS [6]. A secondary beam of  
743  $^{63}\text{Co}$  was selected and allowed to pass through a num-  
744 ber of FRS detectors, the LYCCA ToF start scintilla-  
745 tor and the LYCCA target detectors, which consist of  
746 the target diamond prototype detector and a DSSSD. A  
747 0.4 g/cm<sup>2</sup> thick  $^{197}\text{Au}$  secondary target followed these  
748 detectors. The energy of the  $^{63}\text{Co}$  beam at this point was

749 approximately 165 MeV/u. The beam continued to pass  
750 through the remaining LYCCA ToF Stop scintillator and  
751 LYCCA telescopes before coming to rest in the LYCCA  
752 wall CsI detectors. The flight distances (cf. Fig. 1) were  
753  $d_{in} = 700(5)$  mm and  $d_{out} = 3.61(1)$  m.

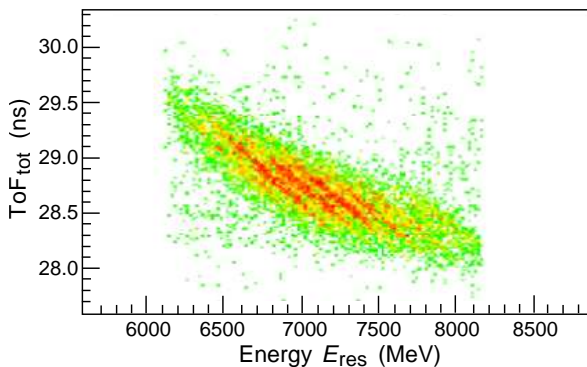


Figure 13:  $\text{ToF}_{tot}$  vs. energy  $E_{res}$  plot showing Fe fragments from the commissioning data.

754 In order to get an idea of the performance of LYCCA,  
755 the mass resolution of Fe fragments, primarily produced  
756 by secondary beam interactions with the diamond de-  
757 tector and DSSSD at the target position, was evaluated.  
758 Using this measurement and knowledge of the energy  
759 resolution, the timing resolution was extracted and all  
760 resolution values were compared with those used in the  
761 LYCCA simulations [10] and outlined in the LYCCA  
762 TDR [11].

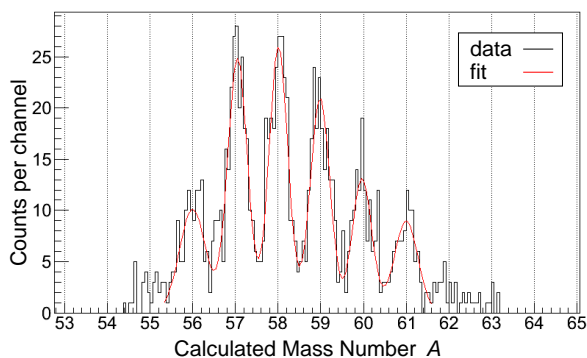


Figure 14: Fe fragment masses calculated on an event-by-event basis. The mass resolution of  $\Delta A = 0.55$  (FWHM) was determined from the average width of the six peak Gaussian least squares fit shown.

A Z = 26 selection was made using  $\Delta E - E_{res}$  data from the LYCCA wall DSSSDs and CsI detectors respectively, as can be seen in Fig. 12. Isotopic identification of the Fe fragments could then be provided by



767 the  $\text{ToF}_{\text{tot}}$  measurements between LYCCA start and stop  
 768 scintillators, as well as the  $E_{\text{res}}$  measurements from the  
 769 LYCCA wall detectors. Only one central  $\Delta E$ - $E_{\text{res}}$  wall  
 770 module was used throughout the analysis to guarantee  
 771 that partially insufficient calibration data did not com-  
 772 promise the mass resolution measurements. Projectile  
 773 tracking using the target and wall DSSSDs allowed po-  
 774 sition corrections to be made to the LYCCA scintilla-  
 775 tors, which improved the accuracy of the timing mea-  
 776 surements [24].

777 The resulting  $\text{ToF}_{\text{tot}}$  vs.  $E_{\text{res}}$  histogram is shown in  
 778 Fig. 13, and can be compared with the simulated plot  
 779 for fragments  $^{50}\text{Fe}$  to  $^{53}\text{Fe}$  in Ref. [10], i.e. in a sim-  
 780 ilar  $Z$  and  $A$  regime and comparable particle energies  
 781 and flight distances. At least four Fe isotopes can be  
 782 identified from the experimental data in Fig. 13. The  
 783 separation between neighbouring 'diagonal lines', i.e.  
 784 neighbouring isotopes, is topologically very similar to  
 785 expectations from the simulations in Ref. [10].

786 The time-of-flight between the target and the LYCCA  
 787 wall,  $\text{ToF}_{\text{out}}$ , and total energy measurements were used  
 788 to calculate fragment masses on an event-by-event ba-  
 789 sis.  $\text{ToF}_{\text{out}}$  was determined from  $\text{ToF}_{\text{tot}}$  using knowl-  
 790 edge of the beam velocity  $\beta$  at various points along the  
 791 beamline, and LYCCA tracking information was used to  
 792 correct for different particle trajectories along the flight  
 793 path. The total energy measurement also required cor-  
 794 rection to ensure that energy losses in the stop scintilla-  
 795 tor and the shielding foil were taken into consideration.

796 The result of these calculations for the  $Z = 26$  se-  
 797 lection can be seen in Fig. 14, which also includes a  
 798 restrictive gate on incoming fragments from the FRS.  
 799 An average measurement of the six most prominent  
 800 peaks produced a mass resolution of  $\Delta A = 0.55(3)$   
 801 (FWHM). A timing resolution for the LYCCA ToF sys-  
 802 tem could only be determined by working backwards  
 803 from this mass resolution and taking a known energy  
 804 resolution, which was measured using a  $^{64}\text{Ni}$  beam with  
 805 minimal matter in the FRS beamline. This reduced the  
 806 energy straggling of the beam, allowing an upper limit  
 807 of  $0.69(2)\%$  (FWHM) to be assigned to the energy re-  
 808 solution. With this knowledge, a lower limit to the effec-  
 809 tive timing resolution of  $\Delta t = 72(4)$  ps (FWHM) was  
 810 extracted for the LYCCA timing system, which corre-  
 811 sponds to  $\Delta t = 51(3)$  ps (FWHM) for each timing de-  
 812 tector. Due to coarse position corrections in the present  
 813 analysis and additional energy and position straggling  
 814 of the  $^{63}\text{Co}$  fragmentation beam, this number is about a  
 815 factor of two worse compared to the number achieved in  
 816 a dedicated test with a primary  $^{64}\text{Ni}$  beam in Ref. [24].  
 817 Nevertheless, it still suffices for proper mass resolu-  
 818 tion (cf. Fig. 14). More details of the analysis proce-

819 dure of this commissioning experiment are presented in  
 820 Ref. [37].

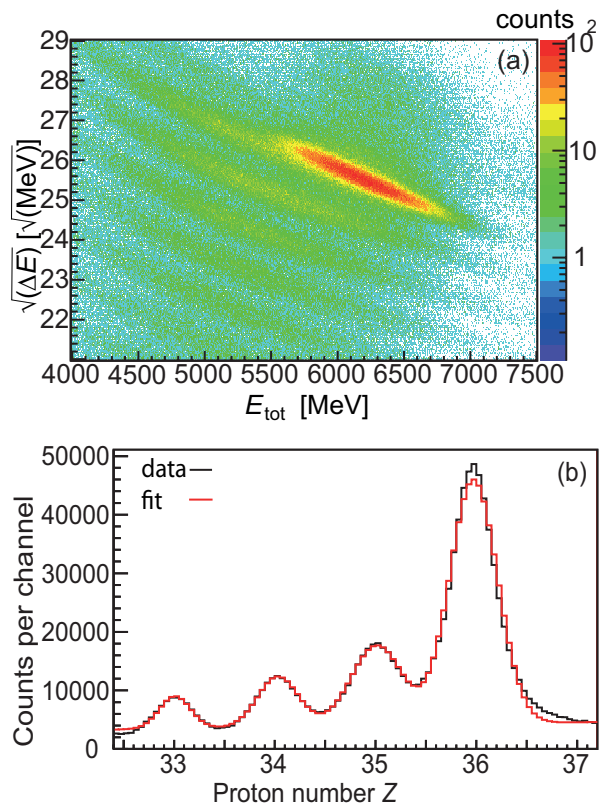


Figure 15: (a) LYCCA  $\sqrt{\Delta E} - E_{\text{tot}}$  plot and (b) charge  $Z$  distribution derived from the energy loss  $\Delta E$  after the secondary target for the  $^{84}\text{Kr}$  fission fragment beam.

In another experiment, a secondary  $^{84}\text{Kr}$  beam was produced by relativistic fission of a  $^{238}\text{U}$  primary beam at 650 MeV/u on a  $^9\text{Be}$  target. This FRS setting on stable  $^{84}\text{Kr}$  was chosen for calibration purposes prior to a Coulomb excitation experiment of the unstable isotope  $^{88}\text{Kr}$ . The experimental set-up was identical to the one of the  $^{63}\text{Co}$  test experiment described above, but with one exception: the prototype diamond ToF detector element was removed.

In Fig. 15(a) the square root of the energy loss in the DSSSD  $\sqrt{\Delta E}$  is plotted versus the total kinetic energy  $E_{\text{tot}}$  deduced from the sum of the energy loss  $\Delta E$  in the DSSSD and the energy  $E_{\text{res}}$  deposited in the CsI. The different nuclear charges from bare ions after the secondary target are clearly separated in this plot. Figure 15(b) shows the  $Z$  distribution obtained from  $\Delta E$  after applying a momentum correction and a  $Z$  calibration (for more details see Ref. [30]) together with a least-square fitted multiple gaussian function. From this fit

840 the charge resolution is calculated to be  $\Delta Z = 0.55$ .

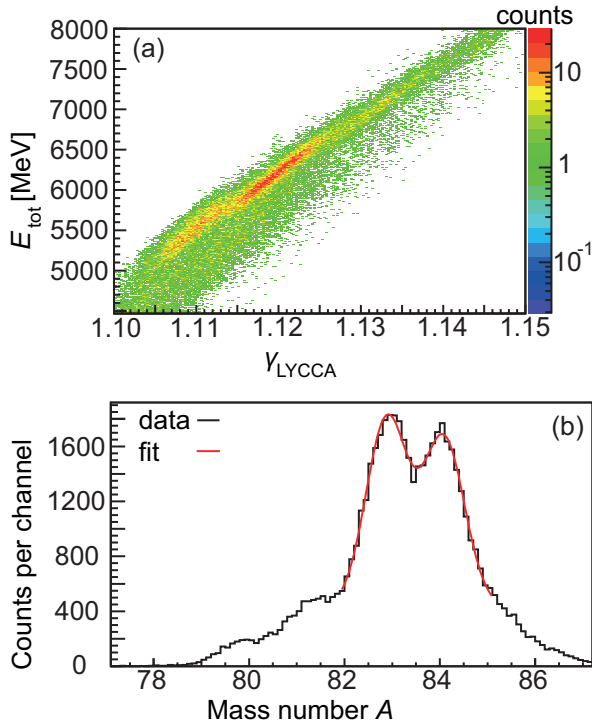


Figure 16: (a) LYCCA  $E_{\text{tot}}$  versus  $\gamma_{\text{LYCCA}}$  plot and (b) mass  $A$  distribution obtained from the distribution (a) by applying a momentum correction, a calibration, and background subtraction. Both plots are in prompt coincidence with incoming  $Z = 35$  fragments using the preceding FRS ion identification.

841 Masses are determined from the correlation between  
 842 total kinetic energy and the time-of-flight. Figure 16(a)  
 843 shows the mass identification plot  $E_{\text{tot}}$  versus  $\gamma_{\text{LYCCA}}$ .  
 844 The relativistic Lorentz factor  $\gamma_{\text{LYCCA}}$  is calculated from  
 845 the ToF measured with LYCCA after the secondary target.  
 846 As a by-product of the  $^{84}\text{Kr}$  beam also bromine isotopes  
 847 can be selected from the incoming beam cocktail  
 848 with a gate on  $Z = 35$  imposed on the FRS ion identifi-  
 849 cation. Following a  $Z = 35$  selection in LYCCA  
 850 as well, the capability of LYCCA to separate the dif-  
 851 ferent Br isotopes after the secondary target is demon-  
 852 strated. The two-dimensional distribution displayed in  
 853 Fig. 16(a) is transformed into the mass spectrum shown  
 854 in Fig. 16(b) by employing a momentum correction, a  
 855 mass calibration, and subtraction of background. For  
 856 a detailed description see Ref. [30]. The distribution  
 857 is least-squares fitted with a multiple gaussian function  
 858 with equal width values. The resulting mass resolution  
 859 (FWHM) for masses  $A \sim 80-85$  yield  $\Delta A = 1.02$ .

860 The preceding – and to some extent still preliminary  
 861 – analyses provide the proof-of-principle of the LYCCA

862 detection scheme. Both energy and timing resolutions  
 863 of the various LYCCA detector elements have to work  
 864 according to or even better than specifications to achieve  
 865 the main characteristics of the set-up, namely

- 866 •  $\Delta Z/Z \lesssim 0.022$  ( $Z \lesssim 26$ ).
- 867 •  $\Delta Z/Z \lesssim 0.015$  ( $Z \lesssim 36$ ).
- 868 •  $\Delta A/A \lesssim 0.010$  ( $A \lesssim 60$ ).
- 869 •  $\Delta A/A \lesssim 0.012$  ( $A \lesssim 80$ ).

870 In the framework of the presently ongoing  
 871 PRESPEC-AGATA campaign at GSI, a compre-  
 872 hensive performance commissioning experiment has  
 873 been performed recently, complemented with extensive  
 874 pulser calibration data. This data is presently being  
 875 analysed. Results concerning LYCCA performance will  
 876 be subject to a forthcoming paper, detailing analysis  
 877 procedures as well as achieved detector, proton number,  
 878 and mass number resolutions [27].

## 879 6. Summary and outlook towards HISPEC at FAIR- 880 NUSTAR

881 The concept, design and prototype developments for  
 882 the FAIR-NUSTAR detector system LYCCA have been  
 883 described. LYCCA aims to discriminate relativistic  
 884 heavy-ion reaction products at typical energies of 100-  
 885 300 MeV/u. Valuable and timely feedback on the LY-  
 886 CCA design concept has been achieved during its early  
 887 PRESPEC implementation of 12- and 16-module pro-  
 888 totype versions of LYCCA at the GSI Helmholtzcentre  
 889 for Heavy Ion Research in the years 2010-2014. With  
 890 the basic LYCCA particle identification concept proven  
 891 (cf. Sec. 5), further optimization on data analysis soft-  
 892 ware algorithms is ongoing [27], and additional detec-  
 893 tors and detector modules as well as electronics up-  
 894 grades are foreseen towards the anticipated implemen-  
 895 tation of the complete LYCCA device for HISPEC ex-  
 896 periments.

897 Concerning detectors, a very-large area plastic scin-  
 898 tillator is being built to cover the approximate full 40-  
 899 cm diameter of the downstream HISPEC beam pipe,  
 900 i.e. the anticipated 26-module version of the LYCCA  
 901 Wall. Concerning these telescopes of the LYCCA Wall,  
 902 the aim is to be able to provide up to 30 CsI blocks  
 903 each of the ‘short’ and ‘long’ version.

904 In terms of read-out and processing electronics, the  
 905 LYCCA Wall telescopes are going to be upgraded to  
 906 already existing and commissioned sampling electron-  
 907 ics modules: for the CsI(Tl)-PD part, the preamplifier

908 signals are going to be digitized with some twenty 16-  
 909 channel GSI-EE FEBEX3 cards [38] based on 14-bit  
 910 50 MHz sampling ADCs. The DSSSDs are going to  
 911 be handled by custom made front-end electronics de-  
 912 veloped in the United Kingdom. It is based on a ap-  
 913 plication specific integrated circuit design for the AIDA  
 914 project [39]. Revised CFD-TDC concepts for the PMT  
 915 signal processing of the large-area scintillators are to be  
 916 investigated.

917 Finally, LYCCA is going to be readily available to  
 918 support physics-driven Super-FRS commissioning to-  
 919 wards FAIR-NUSTAR, either stand-alone or together  
 920 with other FAIR-NUSTAR detectors and activities.

## 921 Acknowledgements

922 LYCCA has been enabled by financial contributions  
 923 of The Swedish Research Council, the German BMBF,  
 924 and the United Kingdom STFC. The Lund group ac-  
 925 knowledges essential additional financial support from  
 926 The Royal Physiographic Society in Lund and The  
 927 Crafoord Foundation in Lund. The LYCCA collabora-  
 928 tion is grateful for the help of in particular GSI staff  
 929 during the first LYCCA commissioning phase.

## References

[1] <http://www.fair-center.eu/for-users/experiments/nustar.html>  
 [2] <http://www.fair-center.eu/en/for-users/experiments/nustar/experiments/hispecdespec.html>  
 [3] <http://www.fair-center.eu/en/for-users/experiments/nustar/experiments/super-frs.html>  
 [4] S. Akkoyun *et al.*, Nuclear Instruments and Methods in Physics Research Section A 668 (2012).  
 [5] P. Boutachkov *et al.*, to be published.  
 [6] H. Geissel *et al.*, Nuclear Instruments and Methods in Physics Research Section B 70 (1992) 286.  
 [7] H.J. Wollersheim *et al.*, Nuclear Instruments and Methods in Physics Research Section A 573 (2005) 637.  
 [8] J. Eberth *et al.*, Nuclear Instruments and Methods in Physics Research Section A 369 (1996) 139.  
 [9] R. Lozeva *et al.*, Nuclear Instruments and Methods in Physics Research Section A 562 (2006) 298.  
 [10] M.J. Taylor *et al.*, Nuclear Instruments and Methods in Physics Research Section A 606 (2009) 589.  
 [11] D. Rudolph *et al.*, LYCCA Technical Design Report, FAIR-NUSTAR, June 2008, available at [http://www.nuclear.lu.se/english/research/basic\\_nuclear\\_physics/nustar/lycca/publications](http://www.nuclear.lu.se/english/research/basic_nuclear_physics/nustar/lycca/publications).  
 [12] <http://www.kns.com>, Kulicke & Soffa, Manual *KS4523 Digital Bonder*.  
 [13] <http://www.bluestarsilicones.com>  
 [14] <http://www.amcrys-h.com>  
 [15] V. Avdeichikov *et al.*, Nuclear Instruments and Methods in Physics Research Section A 349 (1994) 216.  
 [16] V. Avdeichikov *et al.*, Nuclear Instruments and Methods in Physics Research Section A 439 (2000) 158.

[17] V. Avdeichikov *et al.*, Nuclear Instruments and Methods in Physics Research Section A 484 (2002) 251.  
 [18] D. Bédèrede *et al.*, Nuclear Instruments and Methods in Physics Research Section A 518 (2004) 15.  
 [19] A.S. Barann, Bachelor thesis, Lund University, 2013, unpublished.  
 [20] J. Taprogge, Bachelor thesis, Universität zu Köln, 2009, unpublished.  
 [21] V. Avdeichikov *et al.*, Nuclear Instruments and Methods in Physics Research Section A 466 (2001) 427.  
 [22] V. Avdeichikov *et al.*, Nuclear Instruments and Methods in Physics Research Section A 501 (2003) 505.  
 [23] D.D. DiJulio *et al.*, Nuclear Instruments and Methods in Physics Research Section A 612 (2009) 127.  
 [24] R. Hoischen *et al.*, Nuclear Instruments and Methods in Physics Research Section A 654 (2011) 354.  
 [25] F. Schirru *et al.*, J. Instrum. **7**, P05005 (2012).  
 [26] R. Hoischen, PhD thesis, Lund University, LUNFD6 / (NFFR - 1032) / 1-138 / (2011), ISBN 978-91-7473-090-6.  
 [27] LYCCA Collaboration, to be published.  
 [28] P. Moritz *et al.*, Diamond and Related Materials **10**, 1765 (2001).  
 [29] M.Ciobanu *et al.*, IEEE Transactions on Nuclear Science **58** 4 (2011).  
 [30] J. Taprogge, Masters thesis, Universität zu Köln, 2011, unpublished.  
 [31] A. Wendt, PhD thesis, Universitt zu Köln, ISBN 978-3-8439-0860-3 (2013).  
 [32] Phillips Scientific, [www.phillipsscintific.com/](http://www.phillipsscintific.com/)  
 [33] ISEG GmbH, [www.iseg-hv.com/](http://www.iseg-hv.com/)  
 [34] G. Pascovici *et al.*, WSEAS Trans. Circuits and Systems Vol. **7** (6), 470 (2008).  
 [35] B. Kuo and F. Golnaraghi, Automatic Control Systems, John Wiley & Sons Inc., 2003.  
 [36] mesytec GmbH, [www.mesytec.com/](http://www.mesytec.com/)  
 [37] L. Scruton, PhD thesis, University of York, 2013.  
 [38] J. Hoffmann, N. Kurz, S. Loechner, S. Minami, W. Ott, I. Rusanov, S. Voltz and P. Wieczorek, GSI Scientific Report 2011, GSI Report 2012-1 (2012).  
 [39] D. Braga, P.J. Coleman-Smith, T. Davinson, I.H. Lazarus, R.D. Page, and S. Thomas, IEEE Nucl. Sci. Symp. Conf. Record N27-4 (2009); <http://www.ph.ed.ac.uk/~td/AIDA/>.